The influence of nuclear models and Monte Carlo radiation transport codes on stray neutron dose estimations in proton therapy

M. De Saint-Hubert[1*], J. Farah[2], M. Klodowska[3], M. T. Romero-Expósito[4,5], K. Tyminska[6], V. Mares[7], P. Olko[8], L Stolarczyk[8,9] and S. Trinkl[10]

[1] Belgian Nuclear Research Centre (SCK CEN), Boeretang 200, BE-2400 Mol, Belgium.

[2] Institut de Radioprotection et de Sûreté Nucléaire (IRSN), Pôle Radioprotection de l'Homme, BP17, 92260 Fontenay-aux-Roses, France.

[3] Department of Medical Physics and Clinical Engineering, Addenbrooke's Hospital, Hills Road, Cambridge, CB2 0QQ, United Kingdom.

[4] Universitat Autònoma de Barcelona, Departament de Física, E-08193 Bellaterra, Spain.

[5] Instituto Tecnológico de Santo Domingo (INTEC), P.O. Box 342-9/249-2, Santo Domingo, República Dominicana.

[6] National Centre for Nuclear Research, A. Soltana 7, 05-400 Otwock-Swierk, Poland.

[7] Helmholtz Zentrum München, Institute of Radiation Medicine, Ingolstädter Landstraße 1, 85764 Neuherberg, Germany.

[8] Institute of Nuclear Physics PAN, Radzikowskiego 152, 31-342 Krakow, Poland.

[9] The Danish Centre for Particle Therapy, Aarhus University Hospital, Palle Juul-Jensens Boulevard 25, DK-8200 Aarhus, Denmark.

[10] Federal Office for Radiation Protection, Medical and Occupational Radiation Protection, Ingolstädter Landstraße 1, 85764 Neuherberg, Germany.

*corresponding author: mdsainth@sckcen.be

Abstract

Purpose: This study investigates the influence of several Monte Carlo radiation transport codes and nuclear models on the simulation of secondary neutron spectra and its impact on calculating and measuring the neutron doses in proton therapy.

Materials and methods: Three different multi-purpose Monte Carlo radiation transport codes (FLUKA, MCNPX, Geant4) were used together with different available nuclear models, to calculate secondary neutron energy spectra at various points inside a water tank phantom with PMMA walls using a 10 x 10 cm^2 rectangular, mono-energetic proton beam (110 MeV, 150 MeV, 180 MeV, 210 MeV). Using Kerma approximation secondary neutron doses were calculated applying fluence-to-dose equivalent conversion coefficients in water. Moreover, the impact of varying spectra for electrochemically etched CR39 detector calibration was analyzed for different codes and models.

Results: In distal positions beyond the Bragg peak, results show largest variations between the codes, which was up to 53% for the high energy neutron fluence at 16 cm from the Bragg peak of the 110 MeV proton beam. In lateral positions, the variation between the codes is smaller and for the total neutron fluence within 20%. Variation in the nuclear models in MCNPX was only visible for the proton beam energies of 180 and 210 MeV and modeling the high energy neutron fluence which reached up to 23% for 210 MeV at 11 cm lateral from the beam axis. Impact on total equivalent dose was limited for the different models used (<8%) while it was pronounced for the different codes (45% at 16 cm from the Bragg peak of the 110 MeV proton beam). CR39 calibration factors in lateral positions were on average varying 10% between codes and 5 % between nuclear models.

Conclusions: This study demonstrated a large impact on the neutron fluence spectra calculated by different codes while the impact of different models in MCNPX proved to be less prominent for the neutron modeling in proton therapy.

Keywords: Monte Carlo radiation transport codes, nuclear models, neutron dosimetry, CR39, proton therapy.

Highlights:

- Monte Carlo code and nuclear model impact neutron spectra, dose and CR39 calibration
- Codes have larger neutron spectra variation in distal versus lateral positions
- Impact of MCNPX neutron model is only visible for 180 MeV and 210 MeV proton beams
- Calculated total dose equivalent varied up to 45% between the codes
- CR39 calibration factors varied within 10% and 5% between codes and nuclear models

Introduction

In recent years, major technological breakthroughs allowed for more compact and affordable proton therapy units further increasing the number and popularity of such facilities worldwide with more than 66 systems in operation in 2020 and 31 under construction. The physical behavior of protons result in a sharply localized peak of dose, known as the Bragg peak, allowing improved target dose conformation, with reduced entrance and negligible exit dose when compared to other radiotherapy techniques [1]. Nevertheless, one of the challenges of proton therapy is the production of secondary neutrons which are unavoidable due to nuclear interactions of high energy protons with beam line materials and with the patient's body [2]. As therapeutic proton beams have energy of hundreds of MeV and interact with materials of different tissue compositions and densities secondary neutrons, with energies from thermal to high-energy, are inevitably encountered during particle therapy.

Currently, none of the available neutron counters and detectors is fully compatible with a clinical measurement of neutron spectra inside the patient or within an anthropomorphic phantom. Hence, many studies strongly rely on Monte Carlo (MC) particle transport calculations, which are often considered as the reference. The literature extensively reports the use of multiple purpose MC codes such as FLUKA [3-5], MCNPX [6], GEANT4 [7] and PHITS [8] for several applications in proton therapy. First of all, MC codes can be used for out-of-field dosimetry as it allows to compute neutron doses [9-11], which are not considered by the current treatment planning systems used in PT. Furthermore, the shielding of proton therapy facilities is often based on results from MC simulations which allow the computation of neutron ambient dose equivalent [12-14] and the spectral neutron fluence inside and outside the treatment room [15-19].

Only few studies have compared MC simulations to experimental measurements of neutron doses, ambient dose equivalents and Bonner sphere spectrometry in proton therapy (PT) [16, 19-24]. Such studies highlighted large discrepancies between experimental results and MC simulations with up to factors 2-3 presumably due to large measurement uncertainties as well as limitations of nuclear reaction models and cross sections integrated into the MC codes. In general, MC codes allow accurate calculations for neutrons below 20 MeV thanks to existing and well evaluated data libraries, such as ENDF/B [25, 26], which provide reliable neutron cross section data. Above 20 MeV cross-section data are scarce or non-existing for several materials and MC codes. Up to 150 MeV neutrons, MCNP has the ability to utilize data libraries that have recently been released by LANL Group T-2 [27]. Nevertheless, some codes do not use these cross-sections for higher energies and need to rely on nuclear models that describe the interaction of protons and neutrons with target nuclei. Several of these models are available such as Intranuclear Cascade (INC) models (e.g. Bertini, Binary INC model, ISABEL model), pre-equilibrium models as well as evaporation models (e.g. Dresner and Abla). In general, it is difficult to define which of the models are more suitable for simulations in a particular application and for specific elements.

Benchmarking studies have been conducted for heavier elements such as copper and iron [28, 29] but not yet for light elements constituting biological tissues such as hydrogen, oxygen, nitrogen, carbon. Moreover, the influence of MC codes and selection of nuclear models have been tested for Bonner sphere spectrometry (BSS) measurements, as BSS require the input of an initial guess spectrum to start the unfolding process. It was shown that secondary neutron doses from cosmic irradiation as measured with BSS have an uncertainty of 10% related to the different nuclear models and transport codes (GEANT4 and MCNP) [30]. More recently, an even more extended intercomparison of codes (MCNP, MCNPX, FLUKA, PHITS, MARS, or GEANT4) showed an uncertainty of unfolded neutron fluences above 20 MeV of about 20% [31]. Not only BSS and rem counters require MC simulations to assess pre-requisite information for its calibration, also passive detector systems may require MC for energy response correction and/or appropriate calibration. For example, the calibration of electrochemically-etched track detectors (CR39) and the conversion of track density into dose rely on a fluence factor, which is often estimated through MC simulations for a predefined standard neutron source [32, 33] The accuracy and consistency of MC simulations may hence affect experimental measurements by expanding their associated uncertainties and adding up a major component which is currently not quantified.

The European Radiation Dosimetry Group working group 9 (EURADOS WG9) research focusses on the assessment of neutron ambient dose in the proton treatment room and in the facility [34-36] as well as in the patient, more specifically assessing the undesired out-of-field doses during proton therapy [37-39]. Several types of ambient monitors as well as numerous passive detector types have been studied and compared for stray radiation using water and anthropomorphic phantoms. Also comparison of experimental data to MC calculations is often performed, involving the use of many different MC codes and models. Nevertheless, an intercomparison of the different available Monte Carlo codes is missing and needed to assess their performance, identify limitations as well as its impact on the experimental data. This study focused on comparing three widely used MC codes, FLUKA, MCNPX and GEANT4, in the prediction of secondary neutrons following nuclear reactions of a typical proton therapy beam with light elements. The work first involved modeling of a large experimental campaign performed by WG9 [36, 37]. The MC codes were first compared to check their accuracy in reproducing the therapeutic pencil proton beam targeting a 30 x 60 x 30 cm^3 water tank phantom. Next, simulations of neutron spectra inside the water tank phantom were performed at different depths and lateral positions with respect to the Bragg peak and the different fluences were compared. Finally, the variability of neutron spectra among the codes and their impact on experimental measurements was assessed for electrochemically etched CR-39 detectors used in previously conducted experimental campaign [36, 37]. The spectra are needed to determine the calibration factor because in electrochemically etched CR-39 detectors the size of a track does not depend on neutron energy [33].

Materials and Methods

Water phantom and beam parameters

A 30 x 60 x 30 cm³ water phantom with polymethyl methacrylate (PMMA) wall thickness of 15mm and a beam entrance wall with thickness of 4 mm (area 12 x 12 cm^2) was modelled as shown in figure 1. This water phantom was developed by Bordy, et al [40] and used during previously conducted experimental studies within EURADOS WG9 [36, 37]. To investigate the influence of nuclear models on MC particle transport calculations a simple beam model was implemented with four different proton energies of 110 MeV, 150 MeV, 180 MeV and 210 MeV. A 10 x 10 cm² rectangular parallel beam of mono-energetic protons was modelled entering the water phantom at the beam entrance window. Outside the water phantom the beam was travelling through 50 cm of air.

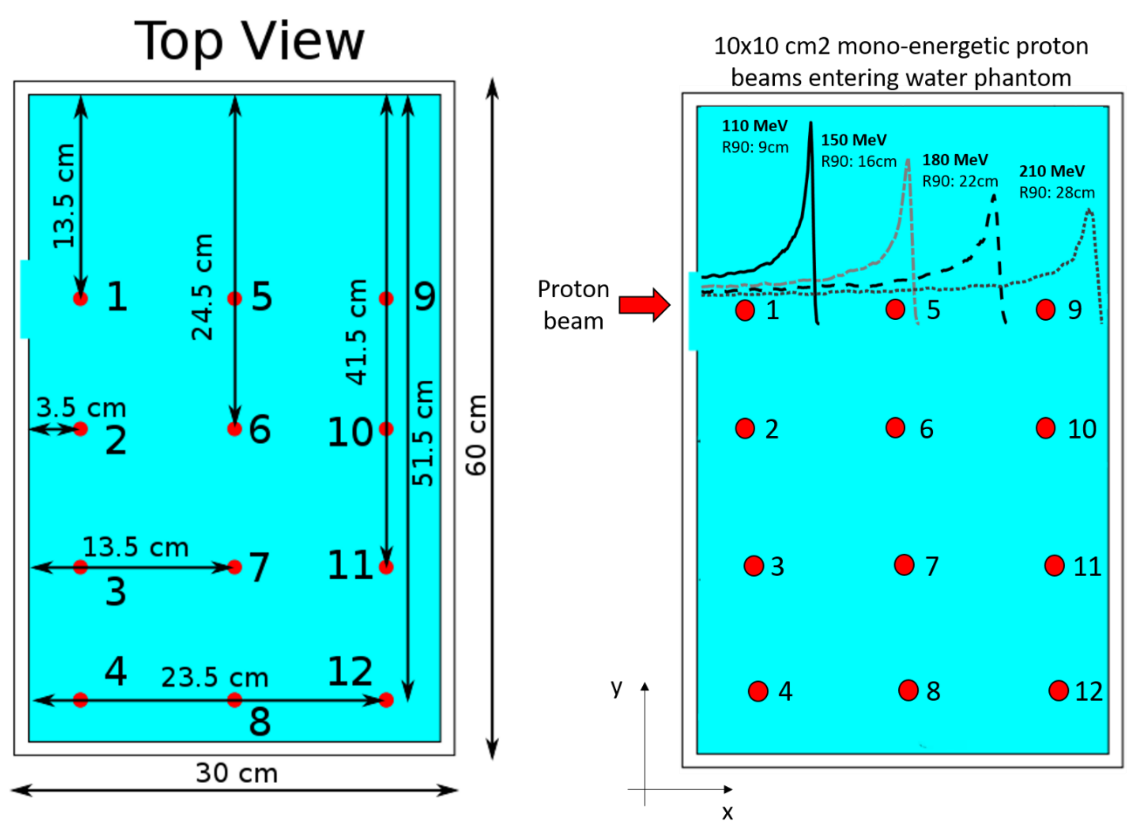

Figure 1. On the left a schematic representation of the 30 x 60 x 30 cm³ water phantom with PMMA walls of 15 mm consisting of a beam entrance window with a thickness of only 4 mm (area 12 x 12 cm²) and 12 different positions (1cm diameter spheres) used for the calculations performed with the different MC simulation codes/models .On the right the entrance of the parallel rectangular 10x10 cm^2 proton beams indicated with

an arrow including Bragg curves for the respective proton energies (MCNPx) demonstrating their different ranges (R90 values) and positions towards the 12 positions in the water phantom.

First, the depth dose distribution for all the four mono-energetic beams was scored using voxelization of the water phantom, with voxel sizes of 1 mm^3. For the definition of range the 90% dose in the distal falloff (R90) values were calculated an we report in this manuscript on the interpolated R90 values for each energies. The distance refers to the distance inside the water phantom (outer wall is set to position zero), thus including a 4mm PMMA wall followed by water (see figure 1).

Furthermore we defined several positions inside the water phantom. In total 12 different positions were defined for comparison of neutron spectra, neutron dose equivalent and CR39 calibration factor. This involved spherical tally volumes of 1 cm diameter (see figure 1).

Table 2. Overview of relative positions towards proton beams for the different mono-energetic proton beams in position 1, 5, 9, 2, 6 and 10. In bold positions that we consider out-of-field, i.e. not within the proton beams Bragg curve. Between brackets the distance towards the Bragg peak (R90) isocenters (0,0) in x and y coordinates as indicated in figure 1.

	Mono-energetic proton beams			
Positions	110 MeV	150 MeV	180 MeV	210 MeV
1	Front Bragg peak (-4,0)	Front Bragg peak (-10,0)	Front Bragg peak (-17,0)	Front Bragg peak (-23,0)
5	**Distal Bragg peak** (6,0)	Bragg peak (0,0)	Plateau Bragg peak (-7,0)	Plateau Bragg peak (-13,0)
9	**Distal Bragg peak** (16,0)	**Distal Bragg peak** (10,0)	**Distal Bragg peak** (3,0)	Plateau Bragg peak (-3,0)
2	**Lateral Bragg peak** (-4,11)	**Lateral Bragg peak** (-10,11)	**Lateral Bragg peak** (-17,11)	**Lateral Bragg peak** (-23,11)
6	**Lateral Bragg peak** (6,11)	**Lateral Bragg peak** (0,11)	**Lateral Bragg peak** (-7,11)	**Lateral Bragg peak** (-13,11)
10	**Lateral Bragg peak** (16,11)	**Lateral Bragg peak** al (10,11)	**Lateral Bragg peak** (3,11)	**Lateral Bragg peak** (-3,11)

The material composition for PMMA and water shown in table 2 were chosen to ensure identical material composition and densitites between codes. Densities were considered for room temperature.

Table 2. Material densities and compositions used for MC calculations

Material	Density (g/cm³)	Isotope	Mass fraction
Air (dry)	0.001205	^{14}N	0.75527
		^{40}Ar	0.01282
		^{16}O	0.23178
		^{12}C	0.00012
Water	0.998	^{16}O	0.33333
		^{1}H	0.66666
PMMA	1.18	^{12}C	0.59985
		^{16}O	0.31962
		^{1}H	0.08054

Monte Carlo codes and nuclear models

Each participant, using a specific Monte Carlo code (1 for GEANT4, 4 for MCNPX and 1 for FLUKA), created dedicated input files for modeling the neutron energy spectra in the different positions in the water phantom. We agreed statistical uncertainties in the bins should be below 5% while for the fluence, dose calculations and calibration factors statistical uncertainties had to remain within 3%.

GEANT4

The binary intra-nuclear cascade model (BIC) [41] was used by setting the standard physics lists QGSP_BIC_HP. Furthermore, the physics list was modified with the electromagnetic physics option 3 and extended for the treatment of thermal neutrons with the G4ThermalNeutronScattering physics. In order to use the thermal scattering physics for hydrogen in water, it was necessary to use TS_H_of_Water defined in G4ThermalNeutronScatteringNames.cc. For all simulations GEANT4 version 10.1.2 was used and neutron energy spectra were simulated.

MCNPX

The Monte Carlo N-Particle eXtended (MCNPX) transport code version 2.7.0 [42] was used in this exercise by 4 different institutes allowing a comparison between the MC output for the same code as implemented by the 4 different groups. The Los Alamos LA150H and LA150N cross section data libraries were used respectively for protons and neutrons [43, 44]. Only for Carbon and Argon model were used for protons due to the missing data tables. Furthermore cross section data libraries are evaluated for about 40 target isotopes and for incident proton energies ranging from 1 MeV to 150 MeV and neutrons from 20 MeV to 150 MeV [45]. Below 20 MeV neutrons and 1 MeV protons endf/b-vii.0 was used. When reaction cross section libraries are not available (> 150MeV), the Bertini intra-nuclear cascade (INC) model [46] and the Dresner evaporation-fission model [47] were used as default. In addition to the default Bertini- Dresner model, different combinations of Bertini and Isabel [48] (for INC modeling) together with Dresner and Abla models (for evaporation phase) were considered. Namely, neutron spectra were simulated for Bert-Dres, Bert-Abla, Isa-Abla and Isa-Dres as well as considering the Cascade-Exciton Model (CEM version 03), combining essential features of the excition and INC models [49, 50]. For a proper evaluation of thermal neutrons, room temperature cross section tables S(a,b) in water (lwtr.10t) were included based on ENDF/B-VII.0 [10].

FLUKA

Physics in FLUKA is unique and unchangeable regardless of chosen settings influencing only code efficiency and calculation precision [51]. For this study, the 2011.2. FLUKA version was used and the HADROTHErapy default settings were applied. This implicates particle transport threshold at 100 keV except for neutrons simulated down to thermal energies [52]. The PEANUT package is incorporated for hadron inelastic nuclear interactions [53] and modified RQMD (Relativistic Quantum Molecular Dynamic) model [54] is employed for nucleus-nucleus interactions between 0.125 and 5 GeV, while below 125 MeV Boltzmann Master Equation (BME) model is used [55].

Neutron dose equivalent calculation from neutron spectra

The impact of modeling the neutron spectra on the simulated neutron dose equivalent quantity for different MC codes and nuclear model was evaluated by using the method explained by Romero-Expósito et al. [32]. Assuming the validity of the kerma approximation, the absorbed dose can be approximated by kerma which, in turn, may be evaluated from neutron fluence through the kerma factors *k(E)* for ICRU tissue found in the work of Siebert and Schuhmacher [56] for neutrons up to 20 MeV and in the work of Chadwick et al up to 150 MeV [44]. Applying the neutron quality factor as a function of energy (*Q(E)*), the neutron dose equivalent can be derived using the following equation:

$$H = \Phi \int_E Q(E) \cdot k(E) \cdot \frac{d\varphi_i(E)}{dE} \cdot dE \qquad (1)$$

where Φ is the total neutron fluence and $\frac{d\varphi_i(E)}{dE}$, the energy spectrum of the unit neutron fluence.

Neutron dose equivalent measurements from CR 39 passive detectors

The basis of dose equivalent evaluation relies in the same equation 1 with a small modification:

$$H = \Phi \int_E Q(E) \cdot k(E) \cdot \frac{d\varphi(E)}{dE} \cdot dE \qquad (2)$$

where Φ is the total neutron fluence, and is obtained by the CR39 passive detector, and $\frac{d\varphi(E)}{dE}$, the energy spectrum of the unit neutron fluence.

As explained in Romero-Expósito et al. [32], total fluence can be evaluated from CR39 reading (*N*) taking into account an average response factor which in turn considers the fractions of each type of neutron in the spectrum:

$$\Phi = \frac{N}{\overline{R_\Phi}} = \frac{N}{p_{epi+th} \cdot R_{epi+th} + p_{fast} \cdot R_{fast} + p_{high} \cdot R_{high}} \qquad (3)$$

being p_{epi+th}, p_{fast}, and p_{high}, the thermal and epithermal fraction, fast fraction, and high energy fraction, respectively, and R_{epi+th}, R_{fast} and R_{high}, the corresponding fluence responses.

Combination of equations 2 and 3 allows to derive the expression used for estimation of the calibration coefficient:

$$\left(H/N\right) = \frac{\int_E Q(E) \cdot k(E) \cdot \frac{d\varphi_i(E)}{dE} \cdot dE}{p_{epi+th} \cdot R_{epi+th} + p_{fast} \cdot R_{fast} + p_{high} \cdot R_{high}} \qquad (4)$$

Results

Benchmarking proton beam

As a first step, a general validation on proton beam ranges was carried out, for all the four mono-energetic beams. In Table 3 the interpolated R90 values from the depth dose distribution are shown in respect to the outer wall of the phantom. A good agreement between the codes was found with the largest differences in R90 value of 1.1 mm for the 180 MeV proton beam. This was considered sufficient for the purpose of this study.

Table 3. R90 values calculated with 3 different Monte Carlo codes (default settings) using 10 x 10 cm² parallel beam of mono-energetic protons.

R90 (cm)	**110 MeV**	**150 MeV**	**180 MeV**	**210 MeV**
GEANT4	8.98	15.62	21.58	28.06
MCNPX	9.01	15.62	21.51	28.07
FLUKA	8.98	15.62	21.47	28.02

Neutron spectra of different MC codes inside the phantom

First we compare the different neutron spectra for the different codes (MCNPX, GEANT4 and FLUKA). For MCNPX we use the default nuclear model (Bert-Dres) and we report on the data of 1 participant.

110 MeV proton beam

Figure 2 shows the results on simulated secondary neutron energy spectra inside the water phantom for 110 MeV at distal positions 5 and 9 and lateral positions 2 and 10.

Tables 4 summarizes the fluence data calculated by the different codes (default models) for 110 MeV at distal positions 5 and 9 and lateral positions 2, 6 and 10 in four neutron energy regions of thermal (E < 0.4 eV), epithermal (0.4 eV < E ≤ 100 keV), fast (100 keV < E ≤ 19.6 MeV) and high energy (E > 19.6 MeV). The thermal neutron fluences varies within 11% while for the fast and high energy neutrons, a strong energy and angular dependency is observed. In the forward scattering directions, i.e. at position 5 and 9, variations in high energy neutron fluence were found up to 46 % and 53 %, respectively, and variations on the total neutron fluence of 16% and 29%, respectively. In lateral positions 2, 6 and 10 the variation on the high energy neutron fluence was found to be lower than in forward directions, up to 12%, 22% and 36%, respectively, while variation on the total neutron fluence was found to be 14%, 6% and 19%, respectively.

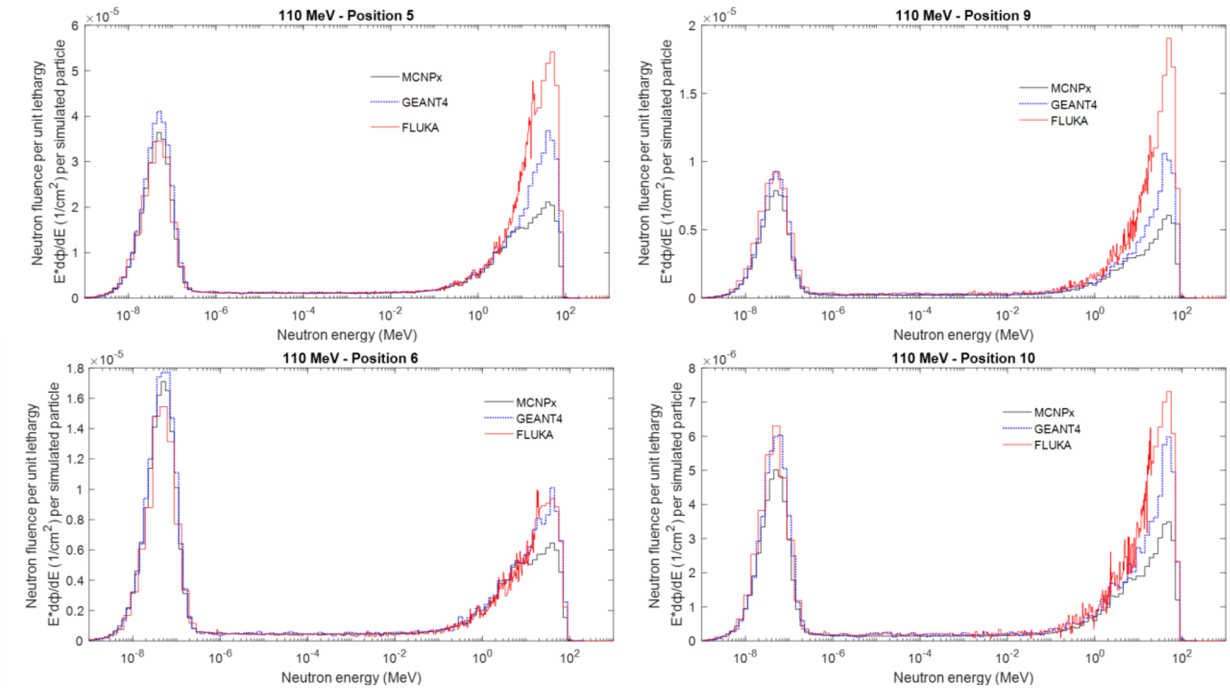

Figure 2. Neutron spectra simulated with different MC codes for 110 MeV proton beam at distal positions 5 and 9 and lateral positions 2 and 10 inside the water phantom.

For comparison the difference to MCNPX was calculated for GEANT4 and FLUKA (see table 4). This was done because MCNPX uses evaluated nuclear cross-sections up to 150 MeV provided in LA150H and LA150N for several materials. Moreover MCNPX has been used by 4 different participants, demonstrating very good agreement, and also particularly since we looked more explicitly into impact of MCNPX models (see section MCNPX intercomparison).

GEANT4 demonstrated a higher thermal neutron fluence compared to MCNPX for all positions except for position 2. This difference was largest for position 10 (17%). FLUKA estimations of the thermal neutron fluence was within 10% for positions 5 and 6 while an underestimation was observed for position 2 (-17%) and an overestimation for positon 9 (25%) and 10 (21%). Moreover, data show that FLUKA largely overestimates the high energy neutrons in forward direction compared to MCNPX. This was 162% in position 5 and up to 200% for position 9. GEANT4 on the other hand also demonstrated an overestimation of the high energy neutron fluence which was up to 72% in position 5.

Table 4. Secondary neutron fluence per simulated particle in distal position 5 and 9 and lateral positions 2, 6 and 10 for 110 MeV proton beam distinguishing between Thermal (E ≤ 0.4 eV), Epithermal (0.4 eV < E ≤ 100 keV), Fast (100 keV < E ≤ 19.6 MeV) and High energy neutrons (E > 19.6 MeV).

		MCNPX	GEANT4		FLUKA		Variation between codes (%)
		Bert-Dres	BIC	Difference to MCNPX	HADROTHE	Difference to MCNPX	
Position 5	Thermal	6.96E-05	7.64E-05	10%	6.84E-05	-2%	6%
	Epith	1.46E-05	1.56E-05	6%	1.51E-05	3%	3%
	Fast	4.42E-05	5.15E-05	17%	6.48E-05	47%	20%
	High	2.39E-05	4.11E-05	72%	6.27E-05	162%	46%
	TOTAL	1.52E-04	1.85E-04	21%	2.11E-04	38%	16%
Position 9	Thermal	1.50E-05	1.71E-05	13%	1.88E-05	25%	11%
	Epith	3.07E-06	3.43E-06	12%	4.28E-06	39%	17%
	Fast	9.16E-06	1.14E-05	24%	1.65E-05	80%	30%
	High	6.74E-06	1.15E-05	70%	2.02E-05	200%	53%
	TOTAL	3.40E-05	4.34E-05	28%	5.98E-05	76%	29%
Position 2	Thermal	4.39E-05	4.30E-05	-2%	3.64E-05	-17%	10%
	Epith	1.03E-05	9.60E-06	-7%	7.29E-06	-29%	17%
	Fast	2.30E-05	2.10E-05	-9%	1.49E-05	-35%	22%
	High	4.09E-06	4.82E-06	18%	3.82E-06	-7%	12%
	TOTAL	8.13E-05	7.84E-05	-4%	6.24E-05	-23%	14%
Position 6	Thermal	3.26E-05	3.41E-05	5%	2.99E-05	-8%	7%
	Epith	5.98E-06	6.33E-06	6%	5.52E-06	-8%	7%
	Fast	1.58E-05	1.77E-05	12%	1.60E-05	2%	6%
	High	7.02E-06	1.01E-05	44%	1.09E-05	55%	22%
	TOTAL	6.14E-05	6.82E-05	11%	6.24E-05	2%	6%
Position 10	Thermal	9.59E-06	1.12E-05	17%	1.16E-05	21%	10%
	Epith	1.95E-06	2.31E-06	19%	2.54E-06	31%	13%
	Fast	5.70E-06	7.20E-06	26%	8.70E-06	53%	21%
	High	3.84E-06	6.21E-06	62%	8.30E-06	116%	36%
	TOTAL	2.11E-05	2.69E-05	28%	3.12E-05	48%	19%

210 MeV proton beam

Figure 3 shows the neutron spectra in lateral positions 2, 6 and 10 of a 210 MeV proton beam, as calculated by the different codes (default models). Table 5 demonstrates an average variation between codes of around 20%, which was uniform across all simulation positions. Data suggest that high energy neutron simulations showed less variation between the codes (14%, 9% and 4% for positions 2, 6 and 10, respectively) when compared to the modeling of lower energy neutrons. Moreover, simulation results at position 10 seem to have better agreement between the codes.

Looking into GEANT4 and FLUKA all these positions showed lower dose estimations when compared to MCNPX except for the high energy neutrons in position 10.

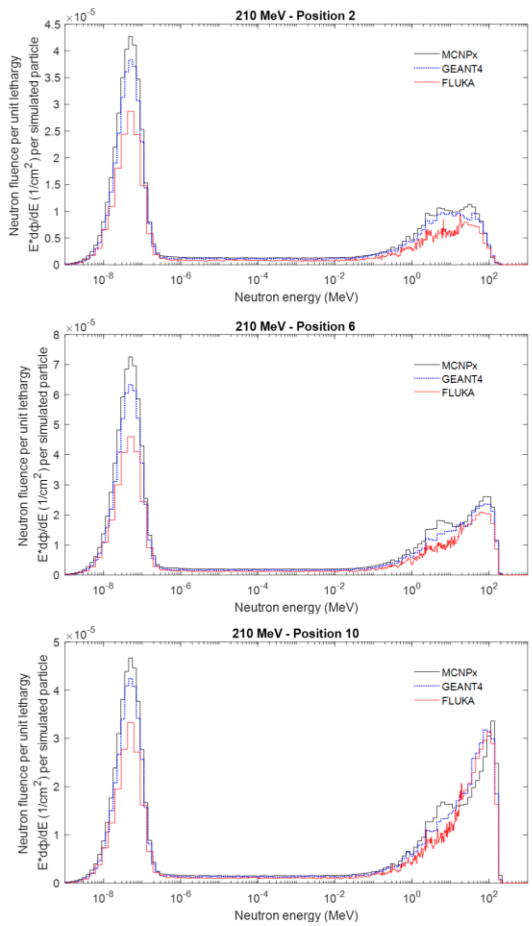

Figure 3. Neutron spectra simulated with different MC codes for 210 MeV proton beams at lateral positions 2 ,6 and 10 inside the water phantom.

Comparison of 110 MeV and 210 MeV proton beams

To compare data for different proton beams at a similar location, comparison of position 2 for 110 MeV (table 4 and 5) with positon 10 for 210 MeV was considered (see table 5). See table 2 for relative x,y positions towards the isocenter (0,0) which is (-4,11) in position 2 for 110 MeV and (-3,11) in position 10 for 210 MeV. Both positions show similar spectral shape (figure 2 down left plot and figure 3 top plot) but the maximum neutron energy is different due to the difference in proton energy.

When comparing variations in the total fluence, these were found to be very similar and limited to 14% for 110 MeV in positon 2 and 12% for 210 MeV in position 10.

In both energies and respective positions, GEANT4 shows lower values than MCNPX for low-energy neutrons and higher values for the high-energy neutrons up to 18% for 110 MeV at position 2. FLUKA tends to underestimate the neutron fluence in both cases resulting in 22 % and 23 % lower values compared to MCNPX for 110 MeV and 210 MeV, respectively, at positions 2 and 10.

Table 5. Secondary neutron fluence per simulated particle in lateral positions 2, 6 and 10 for 210 MeV proton beam distinguishing between Thermal (E ≤ 0.4 eV), Epithermal (0.4 eV < E ≤ 100 keV), Fast (100 keV < E ≤ 19.6 MeV) and High energy neutrons (E > 19.6 MeV).

		MCNPX	GEANT4		FLUKA		Variation between codes (%)
		Bert-Dres	BIC	Difference to MCNPX	HADROTHE	Difference to MCNPX	
Position 2	Thermal	8.18E-05	7.19E-05	-12%	5.53E-05	-32%	19%
	Epith	1.67E-05	1.46E-05	-13%	1.02E-05	-39%	24%
	Fast	3.54E-05	3.16E-05	-11%	2.12E-05	-40%	25%
	High	1.42E-05	1.27E-05	-10%	1.08E-05	-24%	14%
	TOTAL	1.48E-04	1.31E-04	-12%	9.76E-05	-34%	20%
Position 6	Thermal	1.38E-04	1.19E-04	-14%	9.11E-05	-34%	20%
	Epith	2.56E-05	2.15E-05	-16%	1.60E-05	-37%	23%
	Fast	5.74E-05	4.81E-05	-16%	3.52E-05	-39%	24%
	High	4.46E-05	4.13E-05	-7%	3.76E-05	-16%	9%
	TOTAL	2.66E-04	2.30E-04	-14%	1.80E-04	-32%	19%
Position 10	Thermal	8.92E-05	7.95E-05	-11%	6.22E-05	-30%	18%
	Epith	1.97E-05	1.71E-05	-13%	1.36E-05	-31%	18%
	Fast	5.08E-05	4.56E-05	-10%	3.58E-05	-30%	17%
	High	4.96E-05	5.38E-05	8%	5.26E-05	6%	4%
	TOTAL	2.09E-04	1.96E-04	-6%	1.64E-04	-22%	12%

MCNPX intercomparison and evaluation of nuclear models on secondary neutron production

In this study, four different MCNPX implemenations in four different institutes were used. Interestingly all participants used the same version of MCNPX 2.7. and the differences between the fluence spectra as quantified in the different energy windows was within 5% for the same nuclear model settings. Different model configurations were simulated and for proton beam energies of 110 MeV and 150 MeV variation was within 2%, which was expected because of the available cross-sections up to 150 MeV for several elements.

Table 6. Secondary neutron fluence per simulated particle for different MCNPX nuclear models in position 2, 6 and 10 for 180 and 210 MeV proton beam distinguishing between Thermal (E ≤ 0.4 eV), Epithermal (0.4 eV < E ≤ 100 keV), Fast (100 keV < E ≤ 19.6 MeV) and High energy neutrons (E > 19.6 MeV).

		180MeV			Variation between models (%)	**210MeV**			Variation between models (%)
		Bert-Dres	CEM	Isa-Abla		Bert-Dres	CEM	Isa-Abla	
Position 2	Thermal	8.49E-05	8.84E-05	8.69E-05	2%	8.15E-05	9.27E-05	8.56E-05	7%
	Epith	1.77E-05	1.85E-05	1.82E-05	2%	1.66E-05	1.90E-05	1.75E-05	7%
	Fast	3.59E-05	3.72E-05	3.69E-05	2%	3.34E-05	3.90E-05	3.53E-05	8%
	High	1.39E-05	1.06E-05	1.65E-05	22%	1.66E-05	1.25E-05	2.00E-05	23%
	TOTAL	1.52E-04	1.55E-04	1.59E-04	2%	1.48E-04	1.63E-04	1.58E-04	5%
Position 6	Thermal	1.22E-04	1.18E-04	1.22E-04	2%	1.38E-04	1.36E-04	1.33E-04	2%
	Epith	2.29E-05	2.24E-05	2.30E-05	1%	2.55E-05	2.49E-05	2.40E-05	3%
	Fast	5.04E-05	4.71E-05	5.07E-05	4%	5.41E-05	5.34E-05	5.20E-05	2%
	High	3.66E-05	2.96E-05	3.64E-05	12%	4.85E-05	3.39E-05	4.50E-05	18%
	TOTAL	2.32E-04	2.17E-04	2.33E-04	4%	2.66E-04	2.49E-04	2.54E-04	3%
Position 10	Thermal	5.58E-05	5.58E-05	5.57E-05	0%	8.88E-05	8.84E-05	7.99E-05	6%
	Epith	1.17E-05	1.16E-05	1.16E-05	0%	1.95E-05	1.94E-05	1.87E-05	2%
	Fast	3.00E-05	2.82E-05	2.98E-05	3%	4.76E-05	4.49E-05	4.76E-05	3%
	High	3.46E-05	2.97E-05	3.30E-05	8%	5.34E-05	4.31E-05	5.16E-05	11%
	TOTAL	1.32E-04	1.25E-04	1.30E-04	3%	2.09E-04	1.96E-04	1.98E-04	4%

.

Table 6 and figure 4 show neutron fluences obtained with MCNPX simulations considering 3 different combinations of models Bert-Dres, CEM and Isa-Abla for primary proton energies of 180 MeV and 210 MeV at 3 different positions 2, 6 and 10. The effect on the thermal, epithermal and fast neutrons are small with variations within 8%. However, a clear difference between the three considered nuclear models is observed for the high energy neutron fluence. At position 2, the high energy neutron fluence variation between models was 22% and 23% for 180 MeV and 210 MeV protons, respectively. Position 10 shows lower variations in high energy neutron fluence for different nuclear models compared to position 2 with variation of 8% and 11% for 180 MeV and 210 MeV, respectively. In general the variation in models is higher for 210 MeV proton beams compared to 180 MeV protons, except for position 2, where a similar deviation of 22% and 23% for 180 MeV and 210 MeV, respectively, is observed (cf. figure 3 and table 6).

Comparing the three models, it is clear that Bert-Isa-Dres behaves similarly as Isa-Abla, while CEM shows a lower fluence for high energy neutrons.

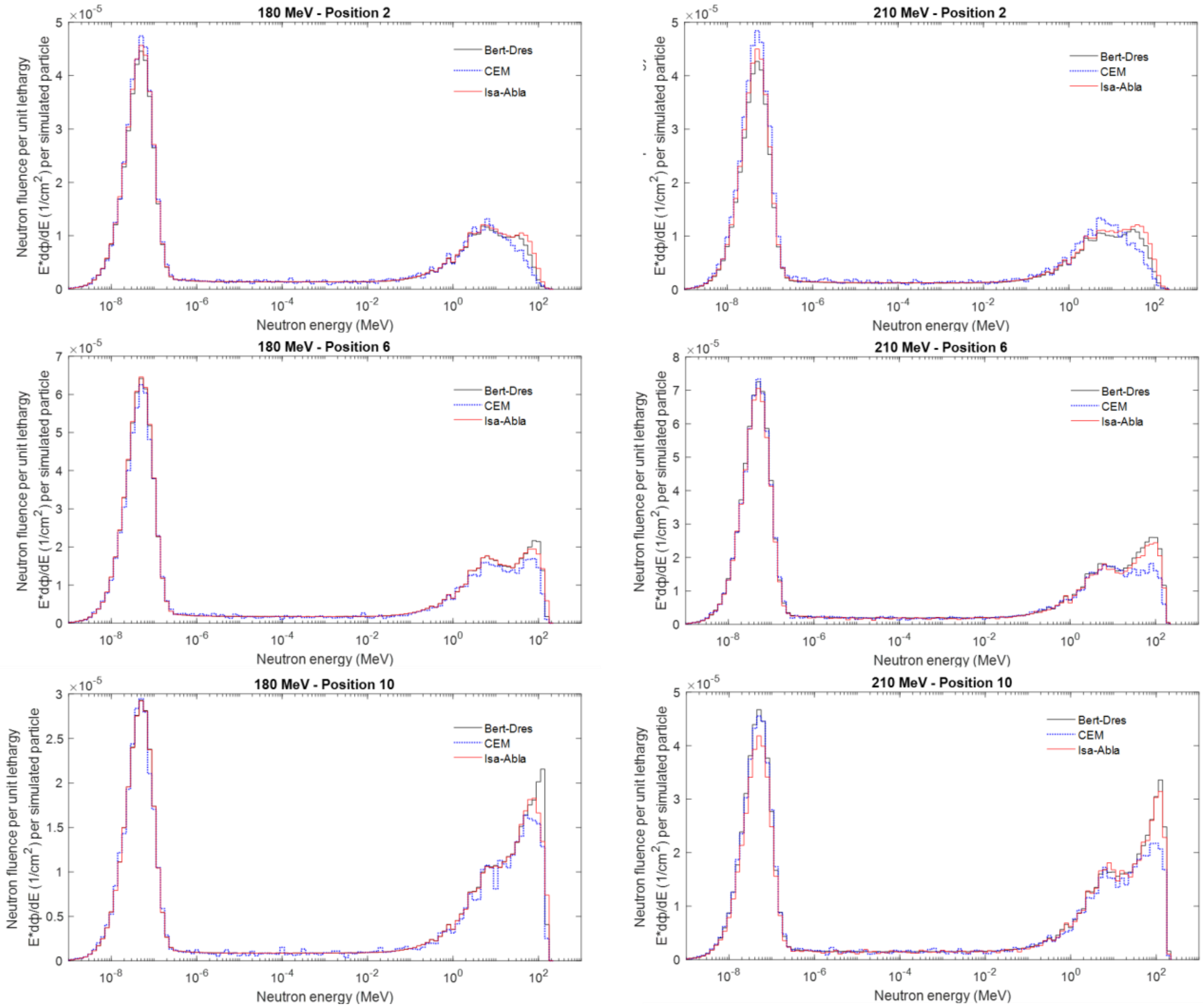

Figure 4. Influence of MCNPX nuclear models on neutron fluence simulated at lateral positions 2 (up), 6 (middle) and 10 (down) considering proton beam energies of 180 MeV (left) and 210 MeV (right).

Impact on calculation of stray neutron dose equivalent

Calculations of the total neutron dose equivalent (mSv/source particle) as calculated on average by the different codes are shown in table 7 together with variations in the total neutron dose equivalent computed by equation (1) and using neutron spectra of the different MC codes at different distal (5 and 9) and lateral (2, 6 and 9) positions for proton beams of 110 MeV, 150 MeV, 180 MeV and 210 MeV. In distal positions variations are generally larger compared to lateral positions and reach up to 45% at position 9 for 110 MeV protons. Obviously due to the different energy spectra and shape of the kerma and quality factors the impact on the equivalent dose (table 7) is different compared to the variation in the total fluence (see table 4 and 5). For 110 MeV we see that the variation on the total neutron dose equivalent is larger than the variation on the total fluence which is not always observed for 210 MeV due to the lower contribution of the high energy neutrons in the spectra (see figure 2 versus figure 3).

Table 7. Average values of total dose equivalent from different MC codes (top) and variation on the total neutron dose equivalent calculated from spectra simulated with different codes (bottom) in distal position 5 and 9 and lateral positions 2, 6 and 10 for 110 MeV, 150 MeV, 180 MeV and 210 MeV proton beams.

Average total dose equivalent [mSv per source particle]				
Position	110 MeV	150 MeV	180 MeV	210 MeV
5	4.31E-11	IF	IF	IF
9	1.14E-11	4.06E-11	9.76E-11	IF
2	9.74E-12	1.40E-11	1.62E-11	1.75E-11
6	1.13E-11	2.35E-11	3.15E-11	3.73E-11
10	5.95E-12	1.68E-11	2.78E-11	4.11E-11
Variation (%) on total dose equivalent between codes				
Position	110 MeV	150 MeV	180 MeV	210 MeV
5	34%	IF	IF	IF
9	45%	32%	25%	IF
2	19%	24%	25%	21%
6	12%	5%	13%	15%
10	30%	16%	7%	5%

IF: in field point

In lateral positions, variations in position 2 was on average 22% for the different proton energies while variation in position 6 was generally lower on average around 11% (ranging between 5% and 15%). The largest variation for lateral positions was observed in position 10 for 110 MeV, which reached up to 30%. This can be explained by the big difference in high energy neutron region of the spectrum related to the fact that position 10 has a small angle towards 110 MeV Bragg peak (35 degrees from the field axis) and so is in a more forward direction than the other lateral positions.

Using different models in MCNPX, the maximum observed relative variation for the total dose equivalent was of 5% (position 2 for 210 MeV).

Impact on experimental evaluation of neutron dose equivalent

The impact of different MC codes and models on the calibration factor of CR39 detectors are shown in table 8 for position 6 and 10 and for different energies. Variation between models was very low and as expected for 110 MeV and 150 MeV proton energies it remained within 1%. For higher proton energies the variation reached up to 8% for 210 MeV in position 6. Variation between codes was on average 10% and 11% for position 6 and 10, respectively.

Table 8. CR39 calibration factors and variation between MCNPX models and MC at lateral positions 6 and 10 for 110 MeV, 150 MeV, 180 MeV and 210 MeV proton beams.

	Proton energy	Bert-Dres	CEM	Isa-Abla	Variation models (%)	GEANT4	FLUKA	Variation codes (%)
Position 6	110 MeV	3.22E-03	3.22E-03	3.22E-03	0%	3.60E-03	3.91E-03	10%
	150 MeV	3.29E-03	3.29E-03	3.29E-03	0%	4.00E-03	4.21E-03	13%
	180 MeV	3.72E-03	3.41E-03	3.70E-03	5%	4.05E-03	4.35E-03	8%
	210 MeV	3.84E-03	3.31E-03	3.77E-03	8%	4.05E-03	4.58E-03	9%
Position 10	110 MeV	3.83E-03	3.88E-03	3.83E-03	1%	4.31E-03	4.65E-03	10%
	150 MeV	4.19E-03	4.19E-03	4.19E-03	0%	4.83E-03	5.33E-03	12%
	180 MeV	4.36E-03	4.10E-03	4.28E-03	3%	5.20E-03	5.44E-03	11%
	210 MeV	4.29E-03	3.99E-03	4.22E-03	4%	4.80E-03	5.52E-03	13%

Discussion

This study focused on comparing three widely used MC codes, FLUKA, MCNPX and GEANT4 in the prediction of secondary neutrons spectra for the assessment of the neutron dose equivalent as well as for calibration of detectors, such as CR39. Firstly, the largest differences in calculating the neutron spectra were observed between different codes and most pronounced in the forward beam direction. Variation between the codes reached up to around 50%, with a maximum disagreement up to 200%, for the high energy neutrons in the forward positions 5 and 9 for 110 MeV. Most likely, this was related to the more prominent high energy component in the forward direction and the lack in cross section data of FLUKA and GEANT4 for neutrons above 20 MeV. MCNPX uses nuclear cross section data until 150 MeV and the present work proved that both FLUKA and GEANT4 tend to overestimate the high energy neutron fluence in forward positions up to 200% for FLUKA (110 MeV position 9) and up to 72% for GEANT4 (110 MeV position 5). For both FLUKA and GEANT4 this overestimation was mostly pronounced in distal positions (behind the Bragg peak) and to a lesser extent at lateral positions 6 and 10 which can be due to the more forwarded direction of these positions towards the Bragg peak for 110 MeV protons with respectively a 60 and 35 degrees angle from the isocenter. Indeed looking into the neutron spectra for 110 MeV proton beam it is clear that position 10 involves an important contribution from high energy neutrons while this is much smaller at position 2.

In lateral positions, variations between the codes for 210 MeV are smaller and less pronounced for the high energy neutrons, reaching up to 20% for the total fluence in position 10. What is noticeable in these lateral positions for 210 MeV protons is that both FLUKA and GEANT4 tend to underestimate the neutron fluence compared to MCNPX.

In general, the performance of the different codes seemed to be related to the relative position and more specifically the angle towards the isocenter. In forward directions an overestimation of FLUKA and GEANT4 is observed while in lateral positions (i.e. lateral position) an underestimation is present (Table 3). This angular dependence is likely due to the contribution/proportion of high energy neutrons prominent at forward directions. Overall the thermal neutron fluence is always most pronounced for GEANT4.

Similarly, the total neutron dose equivalent proved to involve larger variations at distal positions compared to lateral positions. Overall, increasing the proton energy decreased slightly the variation between the codes which is clearly observed in position 9 and 10, respectively, going from 45% for 110 MeV to 25% for 180 MeV and from 30% for 110 MeV to 5% for 210 MeV. Nevertheless, comparison of positions for different energies is challenging as the relative position changes towards the Bragg peak and so does the spectrum and angular distribution. We did compare variation in position 2 for 110 MeV with position 10 for 210 MeV, as these are positions lateral to the Bragg peak, which showed comparable variations. In fact, a limitation of the study is that for the high energy proton beam (210 MeV) we do not have distal positions as the beam ranged up till the end of the water phantom. Nevertheless, the phantom dimensions were based on previous measurements performed in EURADOS WG9 measurement campaigns [37, 40]. Moreover, in realistic clinical conditions an energy of 210 MeV with the range in water exceeding 28 cm is rarely applied. In addition, due to geometrical reasons, proton beam is usually not directed along the patient body so the maximal neutron exposure in forward directions is limited. Therefore, most of out-of-field positions will be lateral to the beam direction as studied in out work.

Besides the impact on the codes, the impact of the choice of the neutron models was tested in MCNPX. We observed only an impact for the 180 and 210 MeV proton beams and for modeling the high energy neutrons which was up to 23% for 210 MeV in position 2. Nevertheless, the impact on the neutron dose equivalent was below 5% and can be considered within the statistical uncertainty for the lateral positions. Interestingly the CEM model showed always lower results than the default model used in MCNPX (Bertini-Dresner) and Isabel-Abla while both Bertini-Dresner and Isabel-Abla show relatively good agreement. Unfortunately, these models could not be validated against measurements, which was beyond the objective of the study. However, in the future EURADOS Working Groups plan to organize validation experiments which could benchmark models and test their performance for this specific application in proton therapy. What is noticeable though is that MCNPX by default uses Bertini-Dresner, while the latest versions of MCNP6.2 uses by default the CEM03 Cascade-Exciton model. Moreover, the pre-equilibrium models used by CEM03, so-called "excition" model, are more extensively developed so it could be considered as a more reliable model. We did not compare the CEM03 model to FLUKA and GEANT4 data and mostly focused to compare the default code setting, but clearly for high proton energies and at lateral positions, we noted overall an underestimation of both FLUKA and GEANT4 towards the default MCNPX model Bertini-Dresner. Finally, when using the spectra for the assessment of the calibration factor of CR39 detectors, we showed the impact is within 10% for the different codes in lateral positions 6 and 10 which reached up to a maximum of 13% for 150 MeV in position 6 and 210 MeV in position 10. The impact of different models reached up to a maximum of 8% for 210 MeV in position 10.

This study describes the uncertainty associated to the MC fluence spectra to assess the calibration factor and can be expected to be around 10% for lateral positions. Compared to the uncertainty associated to the fluence to track density conversion from response factors of 25%, the uncertainty is lower. In previous studies however the combined uncertainty, including this uncertainty with those from track density and MC fluence spectra, was estimated to be around 30%. Unfortunately we were not able to make a direct comparison between simulated data (mono-energetic proton beam) and experimental data (Spread out Bragg peak) from the previous measurement campaign [37], but this is definitely interesting and this work will be continued within EURADOS WG9.

Conclusion

This study demonstrated a significant impact on the neutron fluence spectra calculated by different codes which has an important implication on both the calculated neutron dose equivalent and calibration of CR39 detectors. Use of different nuclear models in MCNPX showed less prominent variations which were only visible for the high energy proton beams and modeling of high energy neutrons, which results in a minor impact on the calculated neutron dose equivalent and calibration of CR39.

Acknowledgements

This work was carried out within EURADOS WG9 - Radiation Dosimetry in Radiohterapy. We would like to thank our colleges for discussion about nuclear models and about existing results of neutron dose measurements inside phantoms.

This research was supported in part by PL-Grid Infrastructure for FLUKA calculations.

References

[1] Hall EJ. Intensity-modulated radiation therapy, protons, and the risk of second cancers. *Int J Radiat Oncol Biol Phys 2006*; 65: 1-7. DOI: 10.1016/j.ijrobp.2006.01.027

[2] Gottschalk B. Neutron dose in scattered and scanned proton beams: in regard to Eric J. Hall (Int J Radiat Oncol Biol Phys 2006;65:1-7). *Int J Radiat Oncol Biol Phys 2006*; 66: 1594; author reply 5. DOI: 10.1016/j.ijrobp.2006.08.014

[3] Pelliccioni M. Overview of fluence-to-effective dose and fluence-to ambient dose equivalent conversion coefficients for high energy radiation calculated using the FLUKA code. *Radiat Prot Dosim 2000*; 88: 279-97. DOI: DOI 10.1093/oxfordjournals.rpd.a033046

[4] Ferrari A, Ranft J and Sala PR. The FLUKA radiation transport code and its use for space problems. *Phys Medica 2001*; 17: 72-80.

[5] Bohlen TT, Cerutti F, Chin MPW, Fosso A, Ferrari A, Ortega PG, et al. The FLUKA Code: Developments and Challenges for High Energy and Medical Applications. *Nucl Data Sheets 2014*; 120: 211-4. DOI: 10.1016/j.nds.2014.07.049

[6] Waters LS, McKinney GW, Durkee JW, Fensin ML, Hendricks JS, James MR, et al. The MCNPX Monte Carlo radiation transport code. *Aip Conf Proc 2007*; 896: 81.

[7] Agostinelli S, Allison J, Amako K, Apostolakis J, Araujo H, Arce P, et al. GEANT4-a simulation toolkit. *Nucl Instrum Meth A 2003*; 506: 250-303. DOI: 10.1016/S0168-9002(03)01368-8

[8] Sato T, Niita K, Matsuda N, Hashimoto S, Iwamoto Y, Furuta T, et al. Overview of particle and heavy ion transport code system PHITS. *Ann Nucl Energy 2015*; 82: 110-5. DOI: 10.1016/j.anucene.2014.08.023

[9] Jiang HY, Wang B, Xu XG, Suit HD and Paganetti H. Simulation of organ-specific patient effective dose due to secondary neutrons in proton radiation treatment. *Phys Med Biol 2005*; 50: 4337-53. DOI: 10.1088/0031-9155/50/18/007

[10] Polf JC and Newhauser WD. Calculations of neutron dose equivalent exposures from range-modulated proton therapy beams. *Phys Med Biol 2005*; 50: 3859-73. DOI: 10.1088/0031-9155/50/16/014

[11] Zheng Y, Newhauser W, Fontenot J, Taddei P and Mohan R. Monte Carlo study of neutron dose equivalent during passive scattering proton therapy. *Phys Med Biol 2007*; 52: 4481-96. DOI: 10.1088/0031-9155/52/15/008

[12] Jarlskog CZ, Lee C, Bolch WE, Xu XG and Paganetti H. Assessment of organ-specific neutron equivalent doses in proton therapy using computational whole-body age-dependent voxel phantoms. *Phys Med Biol 2008*; 53: 693-717. DOI: 10.1088/0031-9155/53/3/012

[13] Taddei PJ, Mirkovic D, Fontenot JD, Giebeler A, Zheng YS, Kornguth D, et al. Stray radiation dose and second cancer risk for a pediatric patient receiving craniospinal irradiation with proton beams. *Phys Med Biol 2009*; 54: 2259-75. DOI: 10.1088/0031-9155/54/8/001

[14] Zheng Y, Fontenot J, Taddei P, Mirkovic D and Newhauser W. Monte Carlo simulations of neutron spectral fluence, radiation weighting factor and ambient dose equivalent for a passively scattered proton therapy unit. *Phys Med Biol 2008*; 53: 187-201. DOI: 10.1088/0031-9155/53/1/013

[15] De Smet V, De Saint-Hubert M, Dinar N, Manessi GP, Aza E, Cassell C, et al. Secondary neutrons inside a proton therapy facility: MCNPX simulations compared to measurements performed with a Bonner Sphere Spectrometer and neutron H*(10) monitors. *Rad Meas 2017*; 99: 25-40. DOI: https://doi.org/10.1016/j.radmeas.2017.03.005

[16] Schneider U, Agosteo S, Pedroni E and Besserer J. Secondary neutron dose during proton therapy using spot scanning. *Int J Radiat Oncol 2002*; 53: 244-51. DOI: Pii S0360-3016(01)02826-7 Doi 10.1016/S0360-3016(01)02826-7

[17] Zheng Y, Newhauser W, Klein E and Low D. Angular Distribution of Neutron Fluence and Its Effect On Shielding for a Passively-Scattered Proton Therapy Unit. *Med Phys 2008*; 35. DOI: 10.1118/1.2962075

[18] Perez-Andujar A, Newhauser WD and DeLuca PM. Contribution to Neutron Fluence and Neutron Absorbed Dose from Double Scattering Proton Therapy System Components. *Nucl Technol 2009*; 168: 728-35. DOI: Doi 10.13182/Nt09-A9297

[19] Hohmann E, Safai S, Bula C, Luscher R, Harm C, Mayer S, et al. INVESTIGATION OF THE NEUTRON STRAY RADIATION FIELD PRODUCED BY IRRADIATING A WATER PHANTOM WITH 200-MeV PROTONS. *Nucl Technol 2011*; 175: 77-80. DOI: Doi 10.13182/Nt11-A12273

[20] Englbrecht FS, Trinkl S, Mares V, Ruhm W, Wielunski M, Wilkens JJ, et al. A comprehensive Monte Carlo study of out-of-field secondary neutron spectra in a scanned-beam proton therapy gantry room. *Z Med Phys 2021*. DOI: 10.1016/j.zemedi.2021.01.001

[21] Tayama R, Fujita Y, Tadokoro M, Fujimaki H, Sakae T and Terunuma T. Measurement of neutron dose distribution for a passive scattering nozzle at the Proton Medical Research Center (PMRC). *Nucl Instrum Meth A 2006*; 564: 532-6. DOI: 10.1016/j.nima.2006.04.028

[22] Farah J, Martinetti F, Sayah R, Lacoste V, Donadille L, Trompier F, et al. Monte Carlo modeling of proton therapy installations: a global experimental method to validate secondary neutron dose calculations. *Phys Med Biol 2014*; 59: 2747-65. DOI: 10.1088/0031-9155/59/11/2747

[23] Farah J, Sayah R, Martinetti F, Donadille L, Lacoste V, Herault J, et al. Secondary Neutron Doses in Proton Therapy Treatments of Ocular Melanoma and Craniopharyngioma. *Radiat Prot Dosim 2014*; 161: 363-7. DOI: 10.1093/rpd/nct283

[24] Stolarczyk L, Cywicka-Jakiel T, Horwacik T, Olko P, Swakon J and Waligorski MPR. Evaluation of risk of secondary cancer occurrence after proton radiotherapy of ocular tumours. *Radiat Meas 2011*; 46: 1944-7. DOI: 10.1016/j.radmeas.2011.05.046

[25] Mosteller RD, Frankle SC and Young PG, *Data Testing of ENDF/B-VI with MCNP: Critical Experiments, Thermal-Reactor Lattices, and Time-of-Flight Measurements*, in Advances in Nuclear Science and Technology, J. Lewins and M. Becker, Editors. 1997, Springer US: Boston, MA. p. 131-95.

[26] Chadwick MB, Obložinský P, Herman M, Greene NM, McKnight RD, Smith DL, et al. ENDF/B-VII.0: Next Generation Evaluated Nuclear Data Library for Nuclear Science and Technology. *Nucl Data Sheets 2006*; 107: 2931-3060. DOI: https://doi.org/10.1016/j.nds.2006.11.001
[27] Little RC, Frankle SC, Hughes IHG and Prael RE. Utilization of new 150-MeV neutron and proton evaluations in MCNP. 1997. United States.
[28] Ferrari A, La Torre FP, Manessi GP, Pozzi F and Silari M. Spallation cross sections for nat Fe and nat Cu targets for 120 GeV/c protons and pions. *Physical Review C 2014*; 0346128980. DOI: 10.1103/PhysRevC.89.034612
[29] Wagner V, Suchopár M, Vrzalová J, Chudoba P, Svoboda O, Tichý P, et al. How to Use Benchmark and Cross-section Studies to Improve Data Libraries and Models. *Journal of Physics: Conference Series 2016*; 724: 012052. DOI: 10.1088/1742-6596/724/1/012052
[30] Pioch C, Mares V and Rühm W. Influence of Bonner sphere response functions above 20 MeV on unfolded neutron spectra and doses. *Radiat Meas 2010*; 45: 1263-7. DOI: https://doi.org/10.1016/j.radmeas.2010.05.007
[31] Rühm W, Mares V, Pioch C, Agosteo S, Endo A, Ferrarini M, et al. Comparison of Bonner sphere responses calculated by different Monte Carlo codes at energies between 1 MeV and 1 GeV – Potential impact on neutron dosimetry at energies higher than 20 MeV. *Radiat Meas 2014*; 67: 24-34. DOI: https://doi.org/10.1016/j.radmeas.2014.05.006
[32] Romero-Expósito M, Domingo C, Sánchez-Doblado F, Ortega-Gelabert O and Gallego S. Experimental evaluation of neutron dose in radiotherapy patients: Which dose? *Med Phys 2016*; 43: 360. DOI: 10.1118/1.4938578
[33] Hälg R, Besserer J, Boschung M, Mayer S, Clasie B, Kry S, et al. Field calibration of PADC track etch detectors for local neutron dosimetry in man using different radiation qualities. *Nuclear Instruments and Methods in Physics Research Section A: Accelerators, Spectrometers, Detectors and Associated Equipment 2012*; 694: 205–10. DOI: 10.1016/j.nima.2012.08.021
[34] Mares V, Romero-Expósito M, Farah J, Trinkl S, Domingo C, Dommert M, et al. A comprehensive spectrometry study of a stray neutron radiation field in scanning proton therapy. *Phys Med Biol 2016*; 61: 4127-40. DOI: 10.1088/0031-9155/61/11/4127
[35] Trinkl S, Mares V, Englbrecht FS, Wilkens JJ, Wielunski M, Parodi K, et al. Systematic out-of-field secondary neutron spectrometry and dosimetry in pencil beam scanning proton therapy. *Med Phys 2017*; 44: 1912-20. DOI: 10.1002/mp.12206
[36] Farah J, Mares V, Romero-Exposito M, Trinkl S, Domingo C, Dufek V, et al. Measurement of stray radiation within a scanning proton therapy facility: EURADOS WG9 intercomparison exercise of active dosimetry systems. *Med Phys 2015*; 42: 2572-84. DOI: 10.1118/1.4916667
[37] Stolarczyk L, Trinkl S, Romero-Expósito M, Mojżeszek N, Ambrozova I, Domingo C, et al. Dose distribution of secondary radiation in a water phantom for a proton pencil beam—EURADOS WG9 intercomparison exercise. *Physics in Medicine & Biology 2018*; 63: 085017. DOI: 10.1088/1361-6560/aab469
[38] Wochnik A, Stolarczyk L, Ambrožová I, Davídková M, De Saint-Hubert M, Domański S, et al. Out-of-field doses for scanning proton radiotherapy of shallowly located paediatric tumours-a comparison of range shifter and 3D printed compensator. *Phys Med Biol 2021*; 66: 035012. DOI: 10.1088/1361-6560/abcb1f
[39] Kneževic Ž, Ambrozova I, Domingo C, De Saint-Hubert M, Majer M, Martínez-Rovira I, et al. COMPARISON OF RESPONSE OF PASSIVE DOSIMETRY SYSTEMS IN SCANNING PROTON RADIOTHERAPY-A STUDY USING PAEDIATRIC ANTHROPOMORPHIC PHANTOMS. *Radiat Prot Dosim 2018*; 180: 256-60. DOI: 10.1093/rpd/ncx254

[40] Bordy JM, Bessieres I, d'Agostino E, Domingo C, d'Errico F, di Fulvio A, et al. Radiotherapy out-of-field dosimetry: Experimental and computational results for photons in a water tank. *Rad Meas 2013*; 57: 29-34. DOI: https://doi.org/10.1016/j.radmeas.2013.06.010
[41] Folger G, Ivanchenko VN and Wellisch J. The Binary Cascade: Nucleon nuclear reactions. *The European Physical Journal A - Hadrons and Nuclei 2004*; 21: 407-17. DOI: 10.1140/epja/i2003-10219-7
[42] Pelowitz DB, MCNPX USER'S MANUAL: Version 2.7.0, in Los Alamos National Laboratory report LA-CP-11-00438. 2011.
[43] Chadwick MB. Neutron, proton, and photonuclear cross-sections for radiation therapy and radiation protection. *Radiat Environ Bioph 1998*; 37: 235-42. DOI: DOI 10.1007/s004110050124
[44] Chadwick MB, Barschall HH, Caswell RS, DeLuca PM, Hale GM, Jones DTL, et al. A consistent set of neutron kerma coefficients from thermal to 150 MeV for biologically important materials. *Medical Physics 1999*; 26: 974-91. DOI: https://doi.org/10.1118/1.598601
[45] Chadwick MB. Nuclear reactions in proton, neutron, and photon radiotherapy. *Radiochim Acta 2001*; 89: 325-36. DOI: DOI 10.1524/ract.2001.89.4-5.325
[46] Bertini HW. *Nucl. Instr. and Meth 1968*; 66.
[47] Dresner LW. *Oak Ridge Report ORNL-TM-196 1962*.
[48] Yariv Y. *Phys. Rev. 1969*; 188.
[49] Gudima KK, Mashnik SG and Toneev VD. Cascade-exciton model of nuclear reactions. *Nuclear Physics A 1983*; 401: 329-61. DOI: https://doi.org/10.1016/0375-9474(83)90532-8
[50] Kerby LM and Mashnik SG. Total reaction cross sections in CEM and MCNP6 at intermediate energies. *Nuclear Instruments and Methods in Physics Research Section B: Beam Interactions with Materials and Atoms 2015*; 356-357: 135-45. DOI: https://doi.org/10.1016/j.nimb.2015.04.057
[51] Robert C, Dedes G, Battistoni G, Bohlen TT, Buvat I, Cerutti F, et al. Distributions of secondary particles in proton and carbon-ion therapy: a comparison between GATE/Geant4 and FLUKA Monte Carlo codes. *Phys Med Biol 2013*; 58: 2879-99. DOI: 10.1088/0031-9155/58/9/2879
[52] FLUKAWebsite. 2005.
[53] Ferrari A and Sala PR. Nuclear reactions in Monte Carlo codes. *Radiat Prot Dosim 2002*; 99: 29-38. DOI: DOI 10.1093/oxfordjournals.rpd.a006788
[54] Sorge H, Stöcker H and Greiner W. Relativistic quantum molecular dynamics approach to nuclear collisions at ultrarelativistic energies. *Nuclear Physics A 1989*; 498: 567-76. DOI: https://doi.org/10.1016/0375-9474(89)90641-6
[55] Cerutti F, Ballarini F, Battistoni G, Colleoni P, Ferrari A, Förtsch SV, et al. Carbon induced reactions at low incident energies. *Journal of Physics: Conference Series 2006*; 41: 212-8. DOI: 10.1088/1742-6596/41/1/021
[56] Siebert B and Schuhmacher H. Quality factors, ambient and personal dose equivalent for neutrons, based on the new ICRU stopping power data for protons and alpha particles. *Radiat Prot Dosim 1995*; 58: 177-83.